nature materials

REVIEW ARTICLE

PUBLISHED ONLINE: 24 JANUARY 2012 | DOI: 10.1038/NMAT3223

Emergent phenomena at oxide interfaces

H. Y. Hwang[1,2,3]*, Y. Iwasa[1,3,4], M. Kawasaki[1,3,4], B. Keimer[5], N. Nagaosa[1,4] and Y. Tokura[1,4,6]*

Recent technical advances in the atomic-scale synthesis of oxide heterostructures have provided a fertile new ground for creating novel states at their interfaces. Different symmetry constraints can be used to design structures exhibiting phenomena not found in the bulk constituents. A characteristic feature is the reconstruction of the charge, spin and orbital states at interfaces on the nanometre scale. Examples such as interface superconductivity, magneto-electric coupling, and the quantum Hall effect in oxide heterostructures are representative of the scientific and technological opportunities in this rapidly emerging field.

Transition metal oxides (TMOs) are ideal for the study of electron correlations, because the transition metal *s* electrons are transferred to the oxygen ions, and the remaining strongly correlated *d* electrons determine their physical properties such as electrical transport, magnetism, optical response, thermal conductivity and superconductivity. These electron correlations constrain the number of electrons at a given lattice site, and induce a local entanglement of the charge, spin and orbital degrees of freedom. This gives rise to a variety of phenomena, for example, Mott insulators, various charge, spin and orbital orderings, metal–insulator transitions, multiferroics and superconductivity[1]. In recent years, there has been a burst of activity to manipulate these phenomena, as well as to create new ones, using oxide heterostructures[2].

A fundamental basis for understanding the physical properties of TMOs is the concept of the symmetry of the order parameter. As Landau recognized, the essence of phase transitions is the change in symmetry. For example, ferromagnetic ordering breaks the rotational symmetry in spin space, that is, the ordered phase has lower symmetry than the Hamiltonian of the system. There are three important symmetries to be considered here. (1) Spatial inversion (I) symmetry, defined as $\mathbf{r} \rightarrow -\mathbf{r}$. In the case of an insulator, breaking this symmetry can lead to spontaneous electric polarization, that is, ferroelectricity, or pyroelectricity once the point group belongs to the polar group symmetry. (2) Time-reversal (T) symmetry defined as $t \rightarrow -t$. In quantum mechanics, the time-evolution of the wavefunction ψ is given by the phase factor $e^{-iEt/\hbar}$ (where E is the energy and $\hbar$ is the reduced Planck constant), hence time-reversal corresponds to taking the complex conjugate of the wavefunction. Additionally, the spin, which is induced by the 'spinning' of the particle, is reversed by time reversal. Broken T symmetry is most naturally associated with magnetism, as the spin operator changes sign with T operation. (3) Gauge (G) symmetry, which is associated with a change (θ) in the phase of the wavefunction as $\psi \rightarrow e^{i\theta}\psi$. G symmetry is connected to the law of charge conservation, and broken G symmetry corresponds to superconductivity or superfluidity.

The interplay among the electronic degrees of freedom produces various forms of symmetry-breaking patterns of I, T and G symmetries, leading to novel emergent phenomena (Fig. 1) that appear only through the collective behaviour of electrons and cannot be expected from individual electrons[3]. From this viewpoint, the interfaces of TMOs offer a unique and important experimental test-bed as I symmetry is broken by the structure itself, and the detailed form of broken I symmetry can often be designed. Also, two-dimensionality usually enhances the effects of electron correlations by reducing their kinetic energy. These two features of oxide interfaces produce many novel effects and functions that cannot be attained in the bulk form. Given that the electromagnetic response is a major source of the physical properties of solids, and new gauge structures often appear in correlated electronic systems, we put 'emergent electromagnetism' at the centre of Fig. 1.

To discuss some basic features of TMOs and their interfaces, Fig. 2a shows a representative crystal structure of TMOs, that is, the perovskite structure. A transition metal ion (M) is surrounded by six oxygen ions, which produce a crystal field acting on M with cubic symmetry. As a consequence, the originally five-fold degenerate 3*d* orbitals are split into three-fold degenerate t_{2g} orbitals (*xy*, *yz*, *zx* orbitals), and two-fold degenerate e_g orbitals (x^2-y^2, $3z^2-r^2$ orbitals). These orbitals have a different sign for the wavefunction depending on the radial direction, which sometimes results in the cancellation of the overlap integrals with the *p* orbitals of the O ions between two neighbouring M ions. Figure 2b shows the three cases that survive this cancellation and lead to a non-zero amplitude for hopping between the two orbitals across an interface (*xy* plane). (Note that the hopping occurs owing to second-order processes that use two hops between the *d* orbitals and the O *p* orbitals.) For all other combinations of the orbitals, the hopping matrix element vanishes.

Next we consider correlation effects on each M ion from the Coulomb interaction, where spin and orbital moments are induced, and the exchange interactions between the two M ions across the interface are of fundamental importance. To consider the exchange processes, virtual hopping — the virtual transfer of the electron from the occupied orbital to the higher energy unoccupied orbital — is a central concept. Figure 2c illustrates two of the possible virtual hopping processes (left and middle), and a forbidden case (right). By using these virtual hopping processes twice, the superexchange interactions are mediated (Fig. 2d). In the intermediate virtual states, the two electrons are occupying the same M ion and hence the energy is increased by the on-site Coulomb repulsion. When the two orbitals are the same (Fig. 2d, left), Pauli's exclusion

[1]Correlated Electron Research Group (CERG) and Cross-Correlated Materials Research Group (CMRG), RIKEN-Advanced Science Institute, Saitama 351-0198, Japan, [2]Department of Applied Physics and Stanford Institute for Materials and Energy Sciences, Stanford University, Stanford, California 94305, USA, [3]CREST, Japan Science and Technology Agency (JST), Tokyo 102-0075, Japan, [4]Department of Applied Physics and Quantum-Phase Electronics Center (QPEC), University of Tokyo, Bunkyo-ku, Tokyo 113-8656, Japan, [5]Max Planck Institute for Solid State Research, 70569 Stuttgart, Germany, [6]Multiferroics Project, ERATO, Japan Science and Technology Agency (JST), Tokyo 113-8656, Japan. *e-mail: hyhwang@stanford.edu; tokura@ap.t.u-tokyo.ac.jp

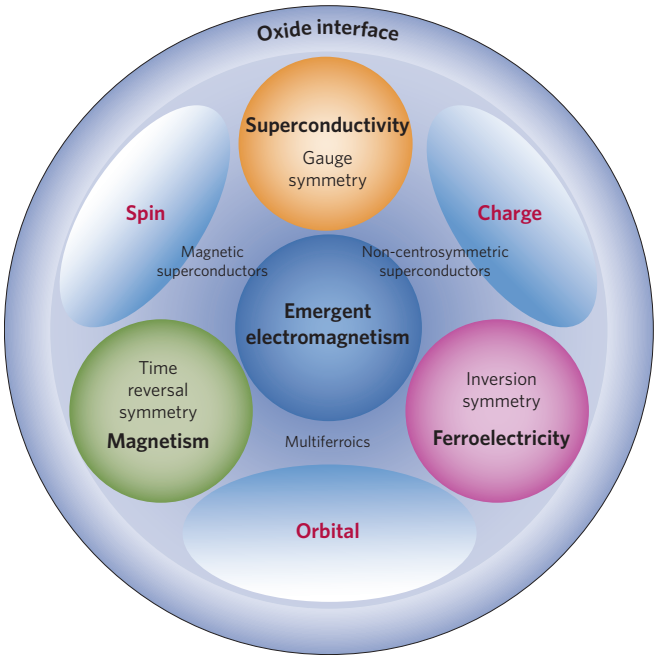

Figure 1 | Schematic diagram showing the symmetries and degrees of freedom of correlated electrons that can be engineered at oxide interfaces.

principle prohibits this second-order process for parallel electron spins resulting in an antiferromagnetic interaction, whereas a ferromagnetic interaction results when the orbitals are different (Fig. 2d, middle). Figure 2d (right) illustrates the ferromagnetic double-exchange interaction mediated by conduction electrons hopping between the two M ions.

Thus far, we have not considered relativistic effects. Consider the electron moving with velocity **v** next to the interface, subject to the electric field **E** due to the broken I symmetry (Fig. 2e). Then in the rest frame of the electron, there appears a magnetic field $\mathbf{B}_{\mathrm{eff}} = \mathbf{v} \times \mathbf{E}$ according to the Lorentz transformation law, which is coupled to the magnetic moment of the electron spin **s** as described by the Hamiltonian $H_{\mathrm{SO}} \propto \mathbf{B}_{\mathrm{eff}} \cdot \mathbf{s} = (\mathbf{v} \times \mathbf{E}) \cdot \mathbf{s}$: this is the relativistic spin–orbit interaction (SOI). When $\mathbf{E} \parallel z$ and $\mathbf{v} \parallel y$, as in Fig. 2e, $\mathbf{B}_{\mathrm{eff}} \parallel x$ and spin precession occurs in the yz plane; this represents the Rashba-type SOI (ref. 4).

With these fundamentals of correlated electrons at interfaces in mind, we describe below how to design and realize various novel functions and phenomena such as charge, orbital and spin reconstructions, magneto-electric coupling, superconductivity and the quantized Hall effect.

Charge, orbital and spin reconstructions

Given that the physical properties of TMOs are often dominated by the state variables of the *d* electrons, a natural starting point for the study of their heterostructures (Fig. 3a) is to determine their configuration at interfaces. Namely, what arrangements of the charge, spin and orbital degrees of freedom can be induced, particularly those that have no bulk analogue? Although some aspects of recent findings have a direct correspondence in semiconductor or metal interfaces, manipulating interface states in TMOs can have striking consequences. It should be noted that the rapid growth of this field has been enabled by fabrication techniques with the prerequisite atomic-scale control, as this is often a very local phenomenon in oxides.

Charge transfer. At any interface between electronic materials, charge can be transferred to equilibrate the electron chemical potential, leading to interface screening in metals, or band bending and depletion in semiconductors. This issue is already more complex for many TMOs, for which the 'semiconductor' or 'metal' is often derived by doping away from a Mott insulator. As this state arises from strong electron interactions, the equivalent of a 'band bending' profile can have much more spatial structure than conventionally understood, reflecting features in the electronic compressibility[5]. Furthermore, the region over which the local carrier density varies can traverse entire phase diagrams, spanning metallic, magnetic and superconducting phases.

An early example of these issues arose in the study of the $CaMnO_3/CaRuO_3$ heterointerface between an antiferromagnetic insulator and a paramagnetic metal[6]. Despite these constituents, the net result is a ferromagnetic interface, from which finite charge transfer between these layers can be deduced. In particular, the ferromagnetic magnetization was found to scale with the number of interfaces, rather than the bulk volume of the constituents. Even in the absence of real charge transfer, geometric control of virtual charge exchange can completely alter the magnetic structure of the interface, following the Kanamori–Goodenough rules for superexchange coupling[7–9].

Subsequently, a number of studies probed the electronic structure of interfaces between materials with different valence states of a given transition metal ion. Figure 3c shows an electron microscopy image of a superlattice composed of $SrTi^{4+}O_3$ and $LaTi^{3+}O_3$, varied down to the level of individual perovskite unit cells[10]. Owing to charge transfer, this heterostructure composed of band insulator and Mott insulator components exhibited metallic behaviour. This can be understood in terms of the nanoscale decomposition of the $(La,Sr)TiO_3$ bulk solid solution, which has been discussed in terms of 'doping' the empty *d* band of $SrTiO_3$ up to half filling[11]. Rather than a strongly disordered average value, local variations in the valence state could be organized and studied for the first time. Furthermore, the region of this variation can be considered to cross the entire bulk phase diagram[11]. However, this occurs in two dimensions only, and as a result of the synthetic opportunities available at interfaces, it is possible to change the balance of competing ground states, or enhance quantum fluctuations, to create new states inaccessible in bulk materials.

Most of the notable bulk physical properties of TMOs arise from doping away from an integer valence state, and thus many studies are examining interfaces between various constituents. For example, $LaMn^{3+}O_3$ and $SrMn^{4+}O_3$ are both antiferromagnetic insulators, but their superlattices exhibit transitions to the ferromagnetic metallic state and associated 'colossal magnetoresistance'[12–14]. Another intriguing system is the interface between insulating La_2CuO_4 and metallic overdoped $(La,Sr)_2CuO_4$. These materials are on either side of the high-temperature superconducting 'dome' of the transition temperature (T_c) versus doping curve, but because of charge transfer, superconductivity is found only at the interface[15,16]. It has been suggested that such a separation of a region of strong pairing potential, and a region of high superfluid density, may be an avenue to enhancing T_c at interfaces[17,18].

Electrostatic boundary conditions in heterostructures. The charge structure of the interface between $LaTiO_3$ and $SrTiO_3$, or $LaMnO_3$ and $SrMnO_3$, actually has two contributions: charge transfer (as discussed previously), and net excess charge owing to the electrostatic boundary conditions imposed. The second aspect can be clearly seen between two perovskites that have different cation sites, and has been most heavily investigated for the $LaAlO_3/SrTiO_3$ interface[19]. Namely, two different interfaces can be formed in the [001] direction — AlO_2–LaO–TiO_2 and AlO_2–SrO–TiO_2 — where the variation lies in the middle atomic layer. This simple degree of freedom has important consequences — the first interface is found to be conducting, whereas the second interface is insulating.

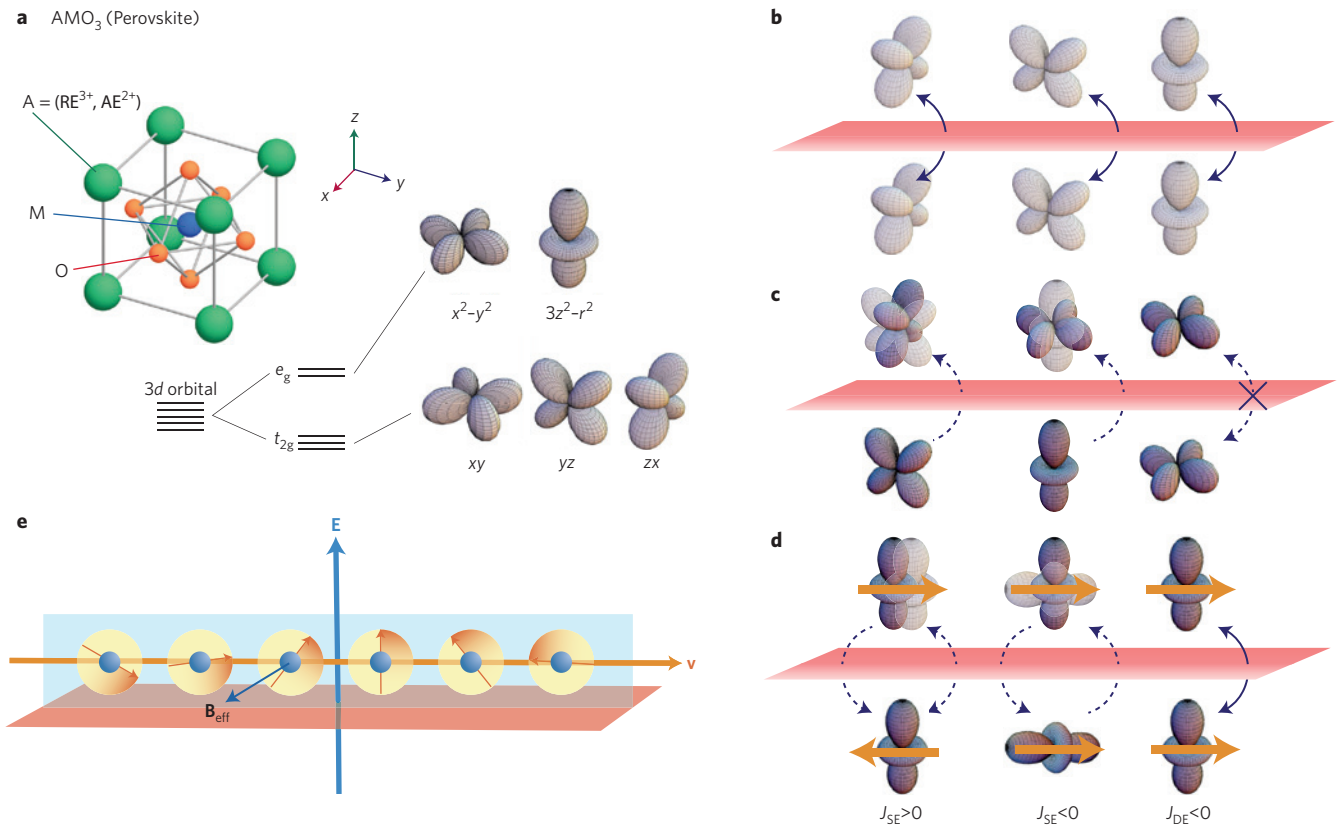

Figure 2 | Orbital and spin configurations at interfaces. a, Perovskite structure and orbital energy levels under the cubic crystal field due to oxygen ions. RE, rare earth elements; AE, alkaline earth elements. **b**, Allowed hopping matrix elements between orbitals across the interface (red). **c**, Allowed virtual hopping matrix elements across the interface. The lightly coloured orbitals are the destination of the virtual hopping process, while the electron is occupied in the darkly coloured orbital. **d**, Various exchange interactions across the interface ($J > 0$, antiferromagnetic; $J < 0$, ferromagnetic); left, antiferromagnetic super-exchange interaction (J_{SE}) using the same orbital in the intermediate state; middle, ferromagnetic super-exchange interaction between different orbitals; right, double-exchange interaction (J_{DE}) where the real hopping of the conduction electron between the two M ions mediates the ferromagnetic coupling. **e**, Rashba-type spin–orbit interaction (SOI); the internal or applied electric field can produce an effective magnetic field (B_{eff}; dark-blue arrow) through the SOI to cause spin precession for the moving electron, or cycloidal spin modulation for localized spins.

In terms of electrostatics, the two choices for the connection between these two insulators impose opposite boundary conditions. In simple ionic terms, $LaAlO_3$ is composed of charged layers of $(La^{3+}O^{2-})^{+}$ and $(Al^{3+}(O^{2-})_2)^{-}$, whereas the corresponding layers in $SrTiO_3$ are charge-neutral. Therefore, terminating the $LaAlO_3$ on an atomic plane at the interface presents the same 'polar catastrophe' that is well-known in surface science to drive reconstructions of polar surfaces, as well as in polar/nonpolar semiconductor heterointerfaces[20,21]. To avoid this diverging interface energy, ±½ compensating charge is required, depending on the interface. The interesting feature of TMOs is their ability to assume different valence states, which can be used to 'create' this compensating charge. For the AlO_2–LaO–TiO_2 interface, Ti^{3+} is observed[22], and this 'electronic reconstruction'[23] can stabilize the interface and source mobile electrons. For the AlO_2–SrO–TiO_2 interface, the source of charge was found to be oxygen vacancies, and here a change in stoichiometry is used for compensation through an 'atomic reconstruction'.

These simplistic ionic considerations have been shown to be robust to varying degrees of covalency, as well as the localized or itinerant nature of the interface charge[24]. Furthermore, they remain present even in real systems with finite interdiffusion. It is suggested that minimizing the electrostatic energy can be a driving force for interface mixing, fundamentally limiting interface abruptness in some cases[22]. However, it should be noted that there is active debate over alternative origins for the interface conductivity that is observed. Perhaps the leading issue is the formation of bulk-like oxygen vacancies in the $SrTiO_3$ near the interface, which provides free carriers[25–27]. There is indeed a very strong dependence of the interface carrier density on the oxygen partial pressure during growth[19,28], or post-annealing, and the degree of intrinsic versus extrinsic contributions to the free carriers is being studied at present. Nevertheless, a clear constraint on all of the bound and free charges of the system is set by the electrostatic boundary conditions, and equilibrated with respect to the electrochemical potential.

An exciting nanofabrication technique that arises from these boundary conditions is the ability to write surface charge using atomic force microscopy, which has been demonstrated to induce conducting features on the nanometre scale[29,30]. This enables access to mesoscopic devices that are competitive with the most advanced electron-beam lithography techniques available. Another direction is to generalize these electrostatic constraints to other interface systems[31]. As shown in Fig. 3, the 'polarity mismatch' is quite general when considering oxide heterostructures with different components. A recent example is shown in Fig. 4, where a quantum well of the Mott insulator $LaVO_3$ is placed in close proximity to the polar $(Al^{3+}(O^{2-})_2)^{-}$ surface of $LaAlO_3$ (ref. 32). Although in isolation, this polar surface reconstructs through oxygen vacancies and lattice distortions[33], on short length scales it can modulation-dope holes in the $LaVO_3$ well[34]. Thus there is a wide variety of doping and valence change schemes that are accessible in heterostructures that do not require local chemical doping, and are therefore free from the strong disorder that is typically introduced in bulk systems.

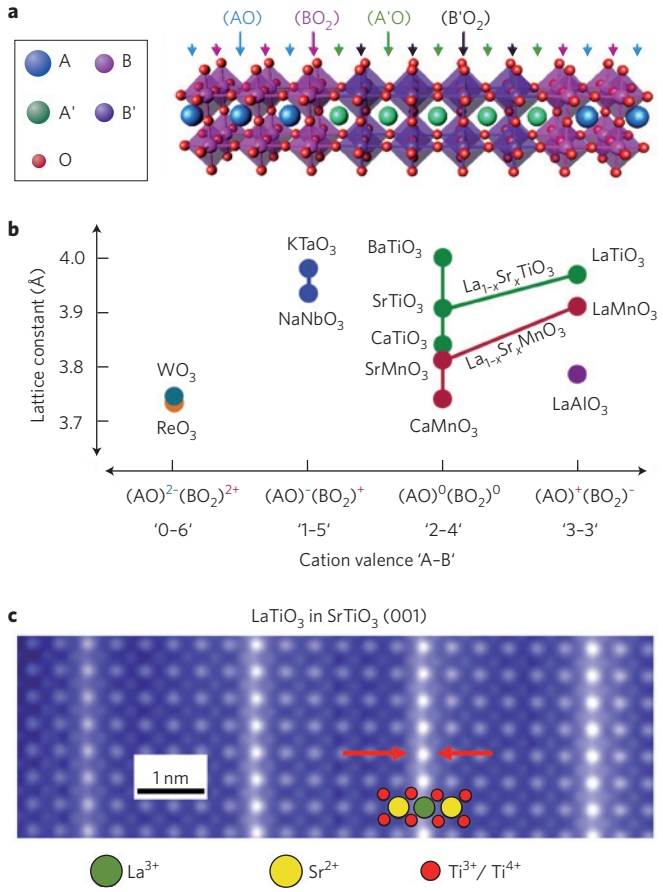

Figure 3 | Atomic and charge structure of pervoskite heterointerfaces. **a**, Schematic of ideal heterointerfaces between two perovskites, ABO_3 and $A'B'O_3$ stacked in the [001] direction. **b**, Representative lattice constants for various perovskites as a function of their charge sequence. **c**, Scanning transmission electron microscopy image of a $LaTiO_3/SrTiO_3$ superlattice[10]. The red arrows show the lanthanum layer. Panel **c**, reproduced from ref. 10, © 2002 NPG.

Spin and orbital reconstructions. In previous sections, we have discussed the rearrangement of charge at oxide interfaces, which is driven primarily by electrostatic interactions. Because of the strong correlation between charge, spin and orbital degrees of freedom, modulations of the charge density in TMOs can easily lead to spin or orbital polarization. One example we have already encountered is the $CaMnO_3/CaRuO_3$ interface, where transfer of a small density of itinerant charge carriers enhances the ferromagnetic double-exchange between Mn spins at the expense of antiferromagnetic super-exchange interactions, and hence induces ferromagnetic spin polarization at the interface[6,35]. An example of charge-driven orbital polarization has been observed at the $LaAlO_3/SrTiO_3$ interface (discussed above) where the polarity mismatch (combined with the incipient ferroelectricity of $SrTiO_3$) induces substantial lattice deformations[36], which subsequently lead to a rearrangement of the level hierarchy of the partially occupied Ti t_{2g} orbitals through crystal-field effects[37].

Another source of orbital and spin polarization in oxide heterostructures is epitaxial strain resulting from the mismatch of the lattice parameters of the TMO constituents. In analogy to the size mismatch between anions and cations in bulk TMOs, this strain is accommodated by a combination of uniform deformations and staggered rotations of the metal-oxide octahedra, which influence the orbital occupation through the crystal field. Lattice deformations resulting from epitaxial strain are ubiquitous in oxide heterostructures and superlattices. Ultrathin TMO films have served as model systems for studies because of their influence on the competition between different spin–orbital ordering patterns in the plane of the film[38,39]. However, unlike the charge-driven reconstructions discussed above, which can be effectively screened at least in metallic or highly polarizable dielectric TMOs, the strain-driven spin and orbital polarization is typically maintained over a spatial range of tens of nanometres.

Directly at the interface, the local crystalline environment of the transition metal ions differs strongly from the bulk-like environment just one unit cell away (Fig. 5). This implies large local differences in both the crystal field and in the network of covalent exchange bonds between metal-ion pairs by bridging oxygen ions. These differences can trigger genuine interfacial 'spin–orbital reconstructions' not secondary to charge rearrangements or epitaxial strain. This type of reconstruction has been predicted[40-44] and observed[45,46] at interfaces between TMOs with partially occupied, nearly degenerate *d* orbitals, such as $LaTiO_3$ or $LaNiO_3$ with a chemically distinct wide-bandgap insulator such as $LaAlO_3$ (Fig. 5). The loss of covalent metal–oxygen–metal bonds at the interface raises the energy of *d* orbitals with lobes pointing towards the interface and leads to preferential occupation of orbitals polarized parallel to the interface.

The opposite effect has been observed at interfaces of superconducting $YBa_2Cu_3O_7$ (refs 47,48) and multiferroic $BiFeO_3$ (ref. 49) with the metallic ferromagnet $La_{0.7}Ca_{0.3}MnO_3$, where new exchange bonds are formed across the interface and induce interfacial orbital and spin polarization. However, these systems are also strongly affected by charge transfer across the interface, which has to be taken into account to arrive at a quantitative description of the experimental results. Other systems with strongly entangled charge, spin and orbital degrees of freedom are interfaces of the orbitally nearly degenerate antiferromagnetic Mott insulators $LaTiO_3$ and $LaVO_3$ with $SrTiO_3$ (as discussed above), where the polarization mismatch between the constituents generates interfacial charge-density profiles that cannot be obtained by chemical substitution in the bulk form. For these systems, novel interfacial charge, spin and orbitally ordered states have been predicted[40,41,50]. Direct observation of the corresponding ordering patterns lateral to the interface remains a challenge for experimental research.

Emergent interface states

As discussed in the previous section, interfaces of TMOs exhibit various interesting properties, ranging from two-dimensional confinement of electronic states that can be naively expected from carrier-doped bulk solid solution analogues, to emergent phenomena that are hard to predict owing to strong correlation effects of *d* electrons as well as reconstructions of their various degrees of freedom. The concomitant presence of two broken symmetries is one of the most intriguing subjects of near-future research of TMO interfaces (Fig. 1). Given that any single interface structurally breaks I symmetry, inducing magnetism or superconductivity is an approach for examining the emergent properties and functionalities of TMO interfaces.

Magneto-electric coupling in tricolour superlattices. Both $CaMnO_3/CaRuO_3$ and $LaMnO_3/SrMnO_3$ interfaces are known to show ferromagnetism owing to the effective doping induced by charge transfer[6,12–14]. However, the magnetization (**M**) induced at a single interface is often too small to be detected by conventional tools, and it is hard to characterize the cross-coupling of **M** with electric polarization (**P**), such as magneto–electric effects. One of the ways to amplify the effect is making superlattices to multiply the signal. In conventional ABAB superlattices, however, **P** has the opposite sign between AB and BA interfaces, which largely cancel each other. In tricolour ABCABC superlattices, all the **P** at the AB

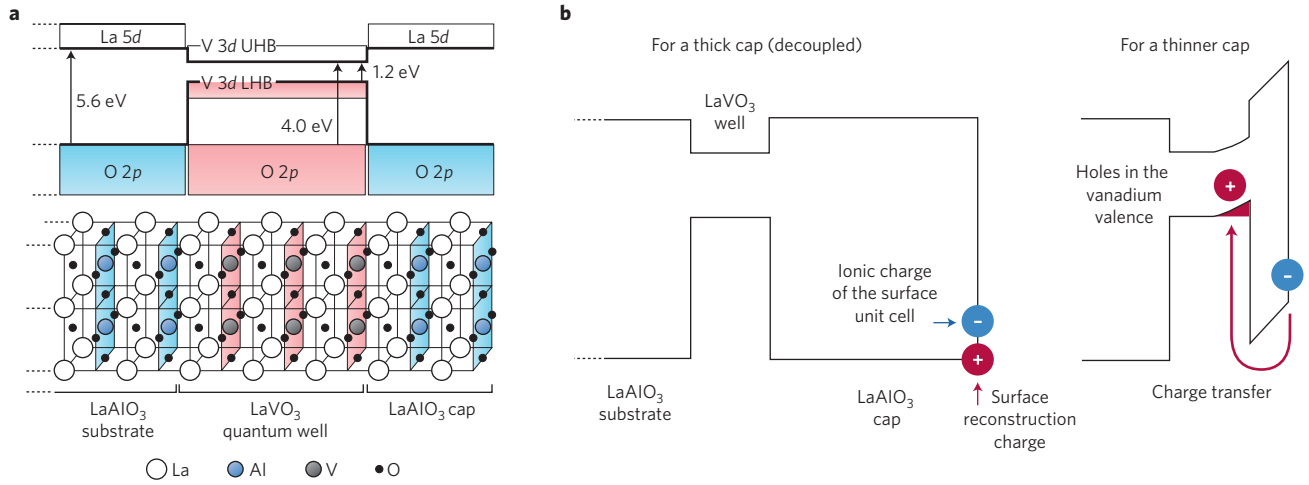

Figure 4 | Modulation doping of holes using polar surfaces. a, Schematic band diagram and crystal structure of a $LaVO_3$ quantum well (red) embedded close to an AlO_2-terminated $LaAlO_3$ (001) surface. UHB, upper Hubbard band; LHB, lower Hubbard band. **b**, Illustrations showing how reconstruction charge at the $LaAlO_3$ surface is transferred to the buried $LaVO_3$ well. To resolve the polar catastrophe of the surface, positive charge is required. When the $LaAlO_3$ cap is thick (left), the surface and the well are electrostatically decoupled, and the positive compensation charge is at the surface. For thinner spacing (right), the $LaVO_3$ well accommodates this positive change, which is energetically more favoured[32,34].

(BC) interfaces can be arranged to have the same sign. In such a case the toroidal moment (**T**) is defined as

$$\mathbf{T} = \frac{1}{2}\sum_i \mathbf{r}_i \times \mathbf{S}_i$$

(here $\mathbf{r}_i$ and $\mathbf{S}_i$ are the electron coordinates and spin components at the ith atomic site, respectively), which remains finite. A non-vanishing toroidal moment is equivalent to a built-in vector potential under the presence of spin–orbit coupling, thereby producing magnetoelectric action.

Accumulating **P** at each interface was predicted and demonstrated in $CaTiO_3/SrTiO_3/BaTiO_3$ ferroelectric–dielectric superlattices to show spontaneous **P** across the entire superlattice[51–53]. By combining ferromagnetic $(La,Sr)MnO_3$ with two different dielectrics, $La^{3+}Al^{3+}O_3$ and $Sr^{2+}Ti^{4+}O_3$, an artificial polar ferromagnet could be constructed[54,55]. A similar or even more straightforward example is isolated interfaces combining $LaMnO_3$ and $SrMnO_3$, which are separated by a third intervening layer of magnetically inactive $LaAlO_3$ (Fig. 6a); $LaMnO_3$ and $SrMnO_3$ are originally antiferromagnets, layered-type and G-type respectively, but their interface becomes ferromagnetic, and polar, due to interface charge-transfer and the resultant double-exchange interaction as discussed above[56]. Here, the concomitant presence of **P** and **T** in these tricolour superlattices is verified using second harmonic (SH) generation and its magneto–optical rotation, respectively. SH generation is rather straightforward; incident laser light with an electric field parallel to the surface (*s* polarization) generates frequency-doubled light with *p* polarization, through the standard nonlinear effect due to **P** perpendicular to the surface. As **T** is orthogonal to both **M** and **P**, by inverting the direction of **M** by applied magnetic field, **T** changes its sign (**P** is invariant, being structurally defined). This in-plane **T** generates a component of *s*-polarized SH response. Combined with the *p*-polarized SH component, this results in Kerr rotation of the SH light, as shown in Fig. 6b.

It is noteworthy in Fig. 6c that the magnitude of **M** as well as the Kerr rotation angle Φ depends critically on the epitaxial strain. This is perhaps related to the effect of orbital reconstruction; the orbital occupation at the ferromagnetic interface prefers the orbital state x^2-y^2 in the case of a tensile-strained interface ($SrTiO_3$ substrate in Fig. 6c), whereas the orbital states x^2-y^2 and $3z^2-r^2$ are degenerate in the cubic case ($La_{0.3}Sr_{0.7}Al_{0.65}Ta_{0.35}O_3$ substrate). The cubic case gives larger **M** (and possibly larger **P**) owing to enhanced charge transfer as shown in Fig. 2, resulting in larger **T** and hence Φ. One of the applications of this technique is to selectively detect ferromagnetic order near the interface. In magnetic tunnel junctions, for example, the important parameter for tunnelling magnetoresistance (TMR) is the spin polarization of charge carriers at the interface. In the case of TMOs, the competition between ferromagnetic and antiferromagnetic order tends to cause spin canting at the interface, which reduces the spin polarization and deteriorates the TMR. This SH technique could detect such a subtle variation of the interface **M** with the change of magnetic field for the $(LaSr)MnO_3/SrTiO_3$

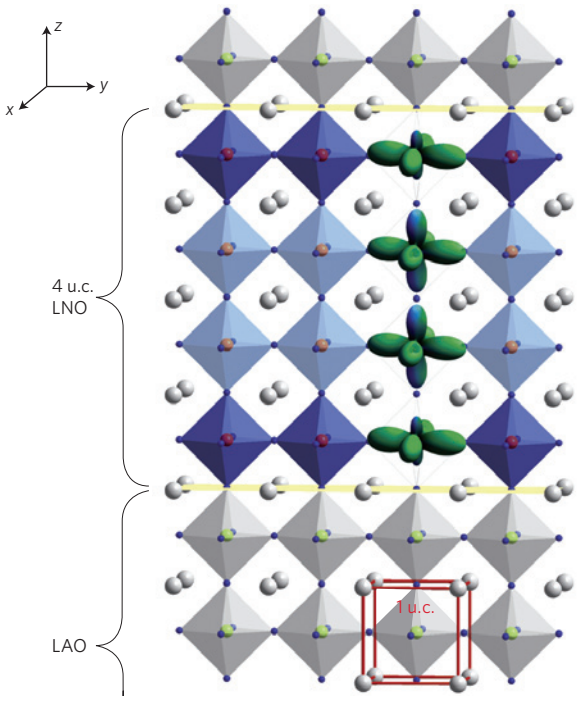

Figure 5 | Heterostructure of metallic $LaNiO_3$ with partially occupied Ni e_g orbitals (LNO, blue) and insulating $LaAlO_3$ (LAO, white)[46]. The orbital polarization at the interface (x^2-y^2 shown in green and $3z^2-r^2$ shown in dark blue) is exaggerated for clarity. Figure reproduced from ref. 46, © 2011 NPG.

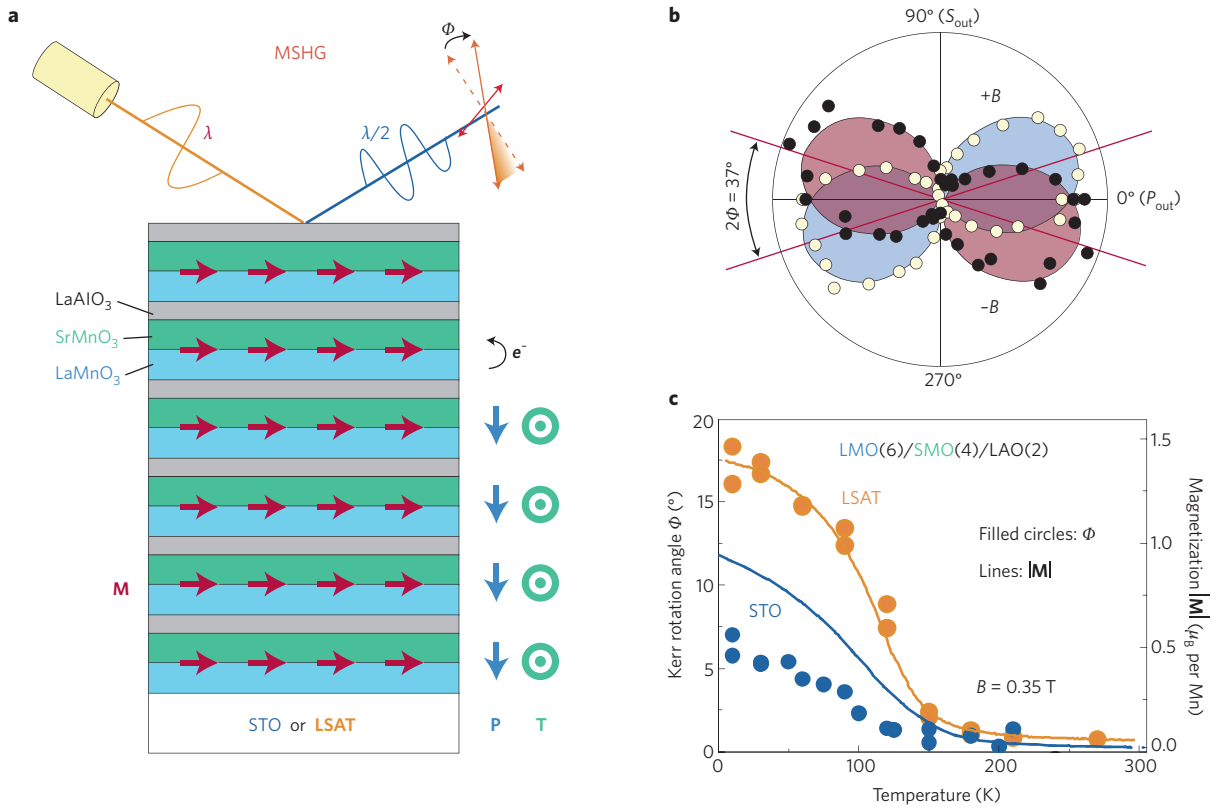

Figure 6 | Magnetization-induced second-harmonic generation (MSHG) for a tricolour superlattice composed of $LaMnO_3$ (LMO), $SrMnO_3$ (SMO), and $LaAlO_3$ (LAO). a, Schematic of the superlattice. For controlling the in-plane lattice strain and resulting preference in orbital occupancy, $La_{0.3}Sr_{0.7}Al_{0.65}Ta_{0.35}O_3$ (LSAT; nearly lattice matched) and $SrTiO_3$ (STO; tensile-strained) substrates were employed. Using incident *s*-polarized fundamental light (λ = 800 nm), the polarization characteristics are analysed for SH light ($\lambda/2$). **b**, Analyser angle dependence of the SH intensity, the white and black filled circles represent a positive and negative applied magnetic field (B) respectively, S_{out} and P_{out} are *s*- and *p*-polarized light respectively. **c**, Kerr rotation angle (Φ; filled circles) and magnetization (lines) of superlattices with the same structure (LMO, six unit cells (u.c.); SMO, four u.c.; LAO, two u.c.) on different substrates. (Data courtesy of Th. Lottermoser, University of Bonn and H. Yamada, AIST).

interface, proving that the overdoping of holes owing to charge transfer biased the ferromagnetic interface towards antiferromagnetism or caused spin canting[57].

Interface superconductivity. Over the past two decades, the creation and control of interface superconductivity in TMOs has attracted growing interest. The most well-known example is the $LaAlO_3/SrTiO_3$ heterostructure (Fig. 7a,e), which is an archetypal 'polar catastrophe' interface. Although both of the two constituent materials are wide-gap insulators, a two-dimensional electron gas (2DEG) is generated at their interface that has a high enough mobility to display quantum oscillations in magnetotransport[19]. Furthermore, this 2DEG exhibits 2D superconductivity at T_c = 0.2 K (ref. 58). This unexpected interface superconductivity is indicative of a further rich variety of emergent properties in TMO interfaces. More importantly, owing to the large dielectric constant of the $SrTiO_3$ substrate, the 2DEG can be modulated by applying a gate voltage (V_G) across the substrate[59,60] (Fig. 7a). The dome-shaped superconducting phase diagram in the T_c–V_G plane obtained on a single device is reminiscent of the $SrTiO_3$ bulk phase diagram[61], demonstrating high tunability of the TMO interfaces.

More versatile gate-tunability is seen in the conventional metal–oxide–semiconductor field-effect transistor (MOSFET) configuration (Fig. 7b). The advantage of electrostatic carrier doping in a MOSFET includes not only high tunability but also absence of chemical disorder, in contrast to chemical doping. The MOSFET structures have been successful in electric-field-control of superconductivity in cuprate ultrathin films[62]. However, superconductivity can be gate-controlled only when it is assisted by chemical doping, because the electrostatically accumulated charge density in MOSFETs is not sufficient for inducing superconductivity in undoped insulators.

Recently, a different type of field-effect device, the electric double-layer transistor (EDLT), was found to have the ability to induce superconductivity in insulators free from chemical doping[63]. A device configuration is illustrated in Fig. 7c. Instead of solid gate dielectrics, the EDLT employs ionic conductors such as electrolytes or ionic liquids. At the semiconductor/electrolyte interface, an electric double layer, a self-organized capacitor with subnanoscale thicknesses, is formed[64]. The working mechanism of EDLTs resembles that of solid gated MOSFETs. The most crucial difference is that V_G predominantly drops at the EDL interface, so that the electric field produced is on the order of 10 MV cm^{-1}, allowing high-density charge accumulation reaching 10^{15} cm^{-2} (ref. 65). This value is 1–2 orders of magnitude larger than that achieved in solid-gated MOSFETs, which are breakdown limited. The application of V_G induced insulator-to-metal transitions followed by superconductivity, as first demonstrated in $SrTiO_3$ (T_c = 0.45 K) (ref. 63), and then in ZrNCl (T_c = 15.2 K) (ref. 66). The concept of the EDLT is quite versatile; in fact, gate tuning of high-T_c cuprates has been already tested[67]. Furthermore, the EDLT technique can be used as a tool for searching for new superconductors.

So far, we have focused on single heterointerfaces including TMOs. However, it should be pointed out that nowadays a variety of artificially designed structures are available in the TMO superstructure systems. An intriguing structure is the δ-doped

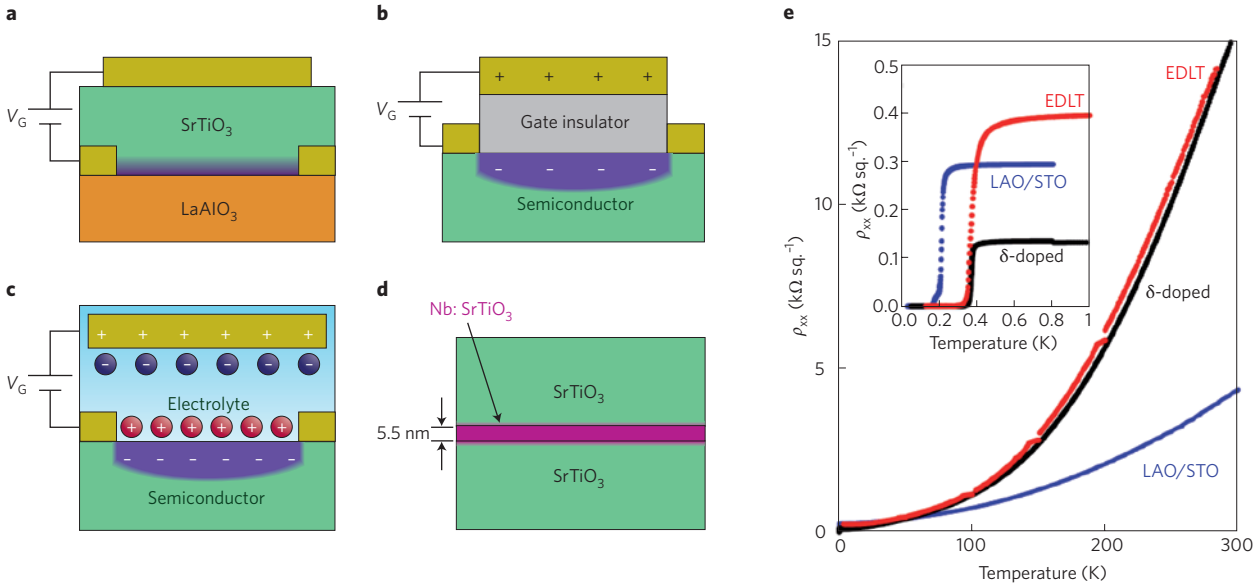

Figure 7 | Various device structures used to produce 2D or interface superconductivity. a, $LaAlO_3/SrTiO_3$ heterostructures with a gate electrode attached on the substrate side of $SrTiO_3$. **b**, MOSFET type device. **c**, EDLT configuration. **d**, δ-doped quantum well using $SrTiO_3$. The 2DEG is indicated in purple. **e**, Comparison of the temperature dependence of the sheet resistance and interface superconductivity of $SrTiO_3$ emerging at the $LaAlO_3/SrTiO_3$ interface (blue)[60], EDLT at $V_G = 3.5$ V (red)[63], and δ-doped quantum well (black)[70]. Inset: magnification of the low temperature region.

quantum well of $SrTiO_3$ (refs 68,69; Fig. 7d), which also displays 2D superconductivity[70]. Here a narrow region of single-crystal $SrTiO_3$ is chemically doped to spatially define a superconducting region. When the width of this region is reduced below the superconducting coherence length, there is a 3D–2D crossover in the superconducting state; similarly, on the de Broglie length-scale, there is a separate dimensional crossover for the normal-state electrons, which exhibit sub-band quantization for narrow channels[71]. Together with the flexibility to vary the local doping level, a rich phase diagram can be engineered to examine superconductor/normal-metal/insulator phase transitions in various dimensions. A notable feature of δ-doping is that the mobility strongly increases in the 2D limit, similar to δ-doping in semiconductors. This aspect suggests that a new regime of 2D superconducting phase transitions can be experimentally accessed approaching the clean limit. Furthermore, bilayer and superlattice structures can be designed to tune interlayer coupling in an artificial analogue of bulk layered superconductors, providing opportunities to address general questions of the role of interlayer coupling in quasi-2D superconductivity.

In addition to controllable carrier density, the interfaces such as $LaAlO_3/SrTiO_3$ and FET devices offer a novel platform for Rashba physics, in which the spin–orbit interaction can be manipulated by the gate electric field[72,73]. At any interface, inversion symmetry is inherently broken, but the gate effects allow us to control the strength of asymmetric potentials, which can be a great advantage for manipulation of spin polarization in TMO interfaces. In this sense, the interface superconductivity in $LaAlO_3/SrTiO_3$ heterostructures as well as in MOSFETs and EDLTs should be further considered as non-centrosymmetric systems. In contrast, the (un-gated) δ-doped structure is inversion symmetric, and thus Rashba effects are excluded.

This contrast is perhaps highly relevant for the recent observations of the microscopic coexistence of ferromagnetism with superconductivity in $LaAlO_3/SrTiO_3$ heterostructures[74–76], which is not found in δ-doped $SrTiO_3$. The fact that these normally antagonistic order parameters can be simultaneously observed indicates that this interface breaks all of the principal symmetries, I, T and G, and with charge[22], orbital[37] and spin reconstructions[28] all at play. It is therefore an intriguing question whether this interface, composed of 'standard' materials, can exhibit exotic superconducting[77] and edge-state phenomena as a result of the formation of an emergent interface state.

Fractional quantum Hall effect in ZnO/(MgZn)O heterostructures. Charge accumulation at oxide interfaces has been used for realizing emergent phenomena as discussed above. When one employs the clean semiconductor ZnO, its 2DEG can exhibit the fractional quantum Hall effect, which is known to emerge only in extremely clean systems such as GaAs (ref. 78). The process of charge accumulation is, in some sense, similar to the polar catastrophe in the $LaAlO_3/SrTiO_3$ system[79]. In $Mg_xZn_{1-x}O/ZnO$ heterostructures, the mismatch in spontaneous polarization of the two piezoelectric compounds is compensated by the charge accumulation at the interface[80]. Electrons are confined in the narrower bandgap material ZnO as shown in inset of Fig. 8a. The first demonstration of the quantum Hall effect in oxides was made possible in a $Mg_{0.15}Zn_{0.85}O/ZnO$ heterostructure fabricated by pulsed laser deposition, which achieved a maximum electron mobility (μ) of 5,500 cm^2 V^{-1} s^{-1} (ref. 80). The use of molecular beam epitaxy has since enabled a great reduction in the impurity concentration of the samples, resulting in a significant μ enhancement[81,82]. Fig. 8a shows an example of the magneto-transport properties for a $Mg_{0.01}Zn_{0.99}O/ZnO$ heterostructure with a charge carrier density $n = 2 \times 10^{11}$ cm^{-2} and $\mu = 300{,}000$ cm^2 V^{-1} s^{-1} that was top-gated[83]. In addition to the integer states ($\nu = 1$, 2 and so on), many fractional states including the most fundamental $\nu = 1/3$ are clearly seen.

Given increasingly higher mobility electrons at oxide interfaces, mesoscopic physics will become a new frontier, where electron coherence lengths exceed device size. For comparison with other semiconductors, we plot in Fig. 8b the transport scattering time $\tau_{tr} = \mu m^*/e$ to represent the cleanness of the systems hosting 2DEGs, where e and m^* are the elementary charge and the electron effective mass, respectively. Given its large m^* and low dielectric constant ε, ZnO displays strong electron correlation effects as characterized by the Wigner–Seitz radius $r_s = 1/\sqrt{\pi n}a^*_B$ where a^*_B is the effective Bohr radius $[(\varepsilon/\varepsilon_0)/(m^*/m_0)]a_B$ (ε_0 is the vacuum permittivity, m_0 is the bare electron mass, and a_B is the Bohr radius). In

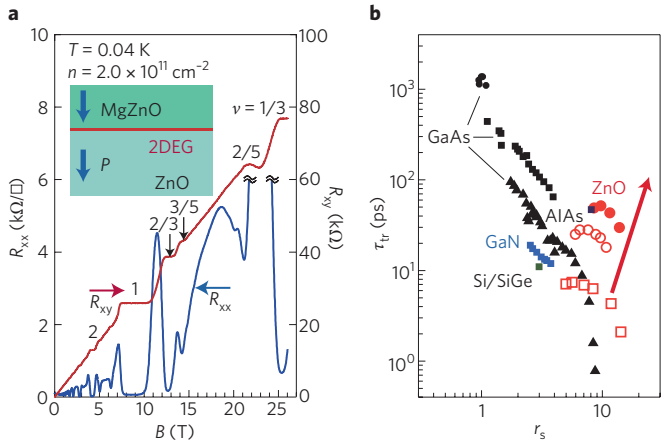

Figure 8 | Fractional quantum Hall effect in ZnO. a, Longitudinal resistance R_{xx} (blue) and Hall resistance R_{xy} (red) of a 2DEG formed at a MgZnO/ZnO interface. Inset: depicts a cross-sectional schematic of the heterostructure. **b**, Comparison of 2DEGs in various semiconductors as functions of the electron–electron interaction strength represented by the Wigner–Seitz radius r_s and transport scattering time τ_{tr}. Data are derived from Fig. 2 of ref. 81 except for the solid red circles, obtained for the sample shown in **a**. The arrow indicates the direction of progress in pursuing a regime of parameters in ZnO that are hard to access in other semiconductors. Panels adapted with permission from: **a**, ref. 83, © 2011 APS; **b**, ref. 81, © 2010 NPG.

current ZnO heterostructures, r_s values have exceeded ten, which is difficult to achieve in other semiconductors while keeping a large τ_{tr}. By improving the growth conditions of ZnO heterostructures and their design, it is possible to reduce the charge-carrier density, further increasing correlation effects, resulting in enhancements of the electron mass and spin susceptibility. A metal–insulator transition is expected in the low n limit; theoretically Wigner crystallization is predicted to occur at r_s over 35 in 2D (ref. 84); in such a situation, new physics may be observed. Incorporating the spin degree of freedom also offers intriguing studies. In fact, the magnetic susceptibility is quite large for 2DEGs in ZnO; the effective g factor (g^*) value is as large as four in contrast to approximately 0.5 in GaAs (ref. 85). Therefore, a quantum Hall ferromagnetic state can be formed[86]. In addition, a ZnO heterostructure is almost free from nuclear spin — the natural abundance of Zn isotopes with non-zero spin (^{67}Zn) is 4%, and that of oxygen with non-zero spin (^{17}O) is 0.038%, and hence the electron–nuclear spin interaction is almost negligible. Therefore, ZnO is an ideal medium for spin-transport experiments. In the same spirit, the spin of a localized electron, for instance in a quantum dot, can be used for storage of quantum information. Finally, ZnO heterostructures can be combined with a variety of material choices in oxides, with the aim of injecting spin-polarized carriers or superconducting Cooper pairs.

Outlook

"The interface is the device," stated Herbert Kroemer in his Nobel address[87]. Although this was in reference to semiconductors, it is particularly important for correlated oxides as well — namely, controlling the interface in terms of atomic, magnetic, orbital and graded-potential design. As described in the preceding sections, TMOs host versatile forms of order in their charge, spin and orbital sectors. These electronic orders meet together at the interface and are strongly affected by electronic processes such as charge transfer, hybridization, and exchange interactions, as well as by the built-in scalar or vector potential, to produce emergent properties and functions. Here, let us briefly discuss possible outcomes of the on-going or near-future research on oxide interfaces in light of Mottronics, orbitronics, spintronics and relativistic electronics.

The term Mottronics was coined to represent electronic functions emerging from the Mott transition, that is, the metal–insulator transition in correlated-electron systems. The interface insulating state can be altered by charge transfer or a gate field to produce a conducting state through the Mott transition. The recently developed ionic-liquid gate method (EDLT) can change the carrier concentration (or band filling) to a larger extent beyond the conventional dielectric solid-state gate and will enlarge the scope for electric-field-induced phase changes at correlated oxide interfaces. An important outcome of this Mottronics is the resistive switching memory function, which can arise from an electric-field-pulse-induced phase change at an interface with a metal electrode. This function may be incorporated in resistance random-access-memory (ReRAM), which is now under development towards industrial applications[88]. One plausible mechanism of the non-volatile resistance switching is the change of the Schottky barrier at the oxide/electrode interface, affected by the current-pulse-assisted movement of oxygen atoms[89]; note here that oxygen stoichiometry is directly related to the d-electron band filling and hence to the metal–insulator phenomena. Another interesting application is the photovoltaic effect at a Mott insulator junction[90] or correlated solar cell. The gradient of potential can be built in for the Mott insulator junction as well as for the conventional semiconductor p–n junction to work as a separator of photogenerated electrons and holes. Multiple carrier generation in the single-photon absorption process may be anticipated in Mott insulator junctions, as already demonstrated for the case of bulk Mott insulators or charge-ordered insulators[91].

The control of the orbital degree of freedom of d electrons is another important subject, and this would lead to orbitronics function. With the change of the orbital state, magnetic, transport and optical properties are significantly altered. In general, interface modification of the magnetic state, for example, in the case of the $LaMnO_3/SrMnO_3$ interface, is inseparable from the orbital state modification. However, even if both phases on either side of the interface are ferromagnetic or metallic, their respective orbital polarizations will strictly gate d-electron hopping across the interface (Fig. 2b,c). Electric-field control or vertical-current switching of the orbital state at the interface will be a good target for the forthcoming orbitronics research. Engineering of spin–orbital Hamiltonians at interfaces may also lead to new routes for high-temperature superconductivity[42,43].

Transition metal oxides often host d-electron magnetism, and hence its interface modulation may lead to spintronics functions. Spin-dependent tunnelling through a barrier layer has been extensively studied in the context of the oxide TMR device, yet researchers have always encountered large modifications of the spin state at the interface even for an originally simple (half-metallic) ferromagnetic state; this easily degrades the TMR characteristics, in particular at elevated temperatures. Conversely, taking advantage of the spin sensitivity to the interface potential, the production of the ferromagnetic state at an oxide interface, say by electric-field gating, will be a challenging subject in the context of spintronics applications. The ferromagnetic moment lying at an interface with broken inversion-symmetry gives rise to the toroidal moment (built-in vector potential), as discussed above. Gate electric-field control of the toroidal moment, if realized, would produce spectacular magnetoelectric functions.

The last, but not least, promising direction is relativistic-electronics, which employs the relativistic SOI. Although this is often an integral component of spintronics in semiconductors and metals, it is only recently being fully appreciated for TMOs, and deserves separate mention. For example in Sr_2IrO_4, spin–orbit splitting is comparable to the on-site Coulomb repulsion, and the insulating state is best described in terms of total angular momentum states[92].

A representative heterostructure effect is the magneto-electric coupling in the spin transistor proposed by Datta and Das[93] where the spin precession is manipulated by the electric field, as well as the spin-galvanic effect, that is, the current-induced spin polarization or the current control of the magnetization[94,95]. When the time-dependence of the SOI is considered, more rich phenomena can be designed, including adiabatic spin pumping and the manipulation of qubits by an electric field. Even without mobile carriers, the coupling between the spin and electric field is induced by the SOI. For example, spin helicity can be controlled by an electric field; through the SOI two non-collinear spins $\mathbf{S}_i$ and $\mathbf{S}_j$ produce the polarization $\mathbf{P} \propto \hat{e}_{ij} \times (\mathbf{S}_i \times \mathbf{S}_j)$ where $\hat{e}_{ij}$ is the unit vector connecting the two spins[96,97]. Therefore, by applying an electric field, the helicity $\mathbf{S}_i \times \mathbf{S}_j$ can in principle be switched.

Even more exotic topological phenomena will be the research targets in the long term. One is the quantized anomalous Hall effect theoretically predicted to occur in 2D metallic ferromagnets, provided that the Hall conductance is larger than $e^2/2h$ while the diagonal conductance is small on this scale[98]. Oxide interface electrons are promising candidates to realize these conditions with careful design of the carrier density and mobility, and the band structure hosting the strong SOI. The other example is the quantum spin Hall system or topological insulator, which is characterized by the nontrivial topological structure of the Bloch wavefunctions in momentum space[99,100]. An interesting direction to pursue in this respect is the interplay between the topology and the electron correlation, for which the electrons at oxide interfaces are promising candidates[101].

Finally, we remark on recent or near-future advances in the experimental means to both prepare and probe the interface electronic state. Underlying these and many related investigations is a direct confrontation of materials chemistry on a microscopic scale. Although the structures described here are metastable, they further require the simultaneous stabilization of components which can require vastly different oxygen potentials in their bulk synthesis. Furthermore, the requirements for interface abruptness are extremely challenging. A variety of state-of-the-art probes of the local electronic structure (such as electron energy-loss spectroscopy[10], resonant X-ray scattering[102] and tomography[103]) generically find that the length-scale for charge transfer is ~1 nm. Thus probing this feature in the intrinsic regime essentially requires atomic-scale control. As for detailed measurements of the electronic structure, angle-resolved photoemission spectroscopy (ARPES) has been an important probe of the quasi-2D electronic state for these decades, and is now evolving into a more bulk-sensitive tool with use of excitations of lower-energy (several-eV laser light) or higher-energy (hard X-ray) light. Thus, ARPES is now applicable to buried interfaces beneath the surface, as well as resonant soft and hard X-ray scattering and absorption spectroscopy. In particular, soft X-ray reflectometry with variable photon energy and polarization can yield atomic-layer-resolved profiles of the charge[104], spin[35] and orbital[46] polarization in oxide heterostructures and superlattices. Other noteworthy advances for potential probes is in spin-polarized neutron reflectometry, detecting the interface magnetic state[105], and the ultra-slow positive muon probe attaining nanometre depth-profile resolution[106]; all will be reinforced by emerging pulsed spallation sources. *In situ* control experiments, for example tracing the change of the interface state while exciting the gate electric field or current, will be of increasing importance in revealing such emergent properties of oxide interfaces.

To conclude, we have discussed the science of oxide interfaces from the viewpoint of emergent phenomena due to strong electron correlations. Combining advances in experimental techniques and new concepts supported by first-principles electronic structure calculations, this system will be an ideal arena for physics, chemistry and technology in the years to come.

References

1. Imada, M., Fujimori, A. & Tokura, Y. Metal–insulator transitions. *Rev. Mod. Phys.* **70,** 1039–1262 (1998).
2. Heber, J. Enter the oxides. *Nature* **459,** 28–30 (2009).
3. Anderson, P. W. More is different. *Science* **177,** 393–396 (1972).
4. Bychkov, Y. A. & Rashba, E. I. Properties of a 2D electron gas with lifted spectral degeneracy. *J. Exp. Theor. Phys. Lett.* **39,** 78–81 (1984).
5. Oka, T. & Nagaosa, N. Interfaces of correlated electron systems: proposed mechanism for colossal electroresistance**.** *Phys. Rev. Lett.* **95,** 266403 (2005).
6. Takahashi, K. S., Kawasaki, M. & Tokura, Y. Interface ferromagnetism in oxide superlattices of $CaMnO_3/CaRuO_3$. *Appl. Phys. Lett.* **79,** 1324–1326 (2001).
7. Goodenough, J. B. Theory of the role of covalence in the perovskite-type manganites [La, *M*(II)]MnO_3. *Phys. Rev.* **100,** 564–573 (1955).
8. Goodenough, J. B. An interpretation of the magnetic properties of the perovskite-type mixed crystals $La_{1-x}Sr_xCoO_{3-\lambda}$. *J. Phys. Chem. Solids* **6,** 287–297 (1958).
9. Kanamori, J. Superexchange interaction and symmetry properties of electron orbitals. *J. Phys. Chem. Solids* **10,** 87–98 (1959).
10. Ohtomo, A., Muller, D. A., Grazul, J. L. & Hwang, H. Y. Artificial charge-modulation in atomic-scale perovskite titanate superlattices. *Nature* **419,** 378–380 (2002).
11. Tokura, Y. *et al.* Filling dependence of electronic properties on the verge of metal–Mott-insulator transitions in $Sr_{1-x}La_xTiO_3$. *Phys. Rev. Lett.* **72,** 2126–2129 (1993).
12. Salvador, P. A., Haghiri-Gosnet, A-M., Mercey, B., Hervieu, M. & Raveau, B. Growth and magnetoresistive properties of $(LaMnO_3)_m(SrMnO_3)_n$ superlattices. *Appl. Phys. Lett.* **75,** 2638–2640 (1999).
13. Yamada, H., Kawasaki, M., Lottermoser, T., Arima, T. & Tokura, Y. $LaMnO_3/SrMnO_3$ interfaces with coupled charge-spin-orbital modulation. *Appl. Phys. Lett.* **80,** 52506 (2006).
14. Bhattacharya, A. *et al.* The metal–insulator transition and its relation to magnetic structure in $(LaMnO_3)_{2n}/(SrMnO_3)_n$ superlattices. *Phys. Rev. Lett.* **100,** 257203 (2008).
15. Gozar, A. *et al.* High-temperature interface superconductivity between metallic and insulating copper oxides. *Nature* **455,** 782–785 (2008).
16. Yuli, O. *et al.* Enhancement of the superconducting transition temperature of $La_{2-x}Sr_xCuO_4$ bilayers: role of pairing and phase stiffness. *Phys. Rev. Lett.* **101,** 057005 (2008).
17. Berg, E., Orgad, D. & Kivelson S. A. Route to high-temperature superconductivity in composite systems. *Phys. Rev. B* **78,** 094509 (2008).
18. Okamoto, S. & Maier, T. A. Enhanced superconductivity in superlattices of high-T_C cuprates. *Phys. Rev. Lett.* **101,** 156401 (2008).
19. Ohtomo, A. & Hwang, H. Y. A high-mobility electron gas at the $LaAlO_3/SrTiO_3$ heterointerface. *Nature* **427,** 423–426 (2004).
20. Baraff, G. A., Appelbaum, J. A. & Hamann, D. R. Self-consistent calculation of the electronic structure at an abrupt GaAs-Ge interface. *Phys. Rev. Lett.* **38,** 237–240 (1977).
21. Harrison, W. A., Kraut, E. A., Waldrop, J. R. & Grant, R. W. Polar heterojunction interfaces. *Phys. Rev. B* **18,** 4402–4410 (1978).
22. Nakagawa, N., Hwang, H. Y. & Muller, D. A. Why some interfaces cannot be sharp. *Nature Mater.* **5,** 204–209 (2006).
23. Hesper, R., Tjeng, L. H., Heeres, A. & Sawatzky, G. A. Photoemission evidence of electronic stabilization of polar surfaces in K_3C_{60}. *Phys. Rev. B* **62,** 16046–16055 (2000).
24. Stengel, M. & Vanderbilt, D. Berry-phase theory of polar discontinuities at oxide-oxide interfaces. *Phys. Rev. B* **80,** 241103(R) (2009).
25. Kalabukhov, A. *et al.* Effect of oxygen vacancies in the $SrTiO_3$ substrate on the electrical properties of the $LaAlO_3/SrTiO_3$ interface. *Phys. Rev. B* **75,** 121404(R) (2007).
26. Siemons, W. *et al.* Origin of charge density at $LaAlO_3$ on $SrTiO_3$ heterointerfaces: possibility of intrinsic doping. *Phys. Rev. Lett.* **98,** 196802 (2007).
27. Herranz, G. *et al.* High mobility in $LaAlO_3/SrTiO_3$ heterostructures: origin, dimensionality, and perspectives. *Phys. Rev. Lett.* **98,** 216803 (2007).
28. Brinkman, A. *et al.* Magnetic effects at the interface between non-magnetic oxides. *Nature Mater.* **6,** 493–496 (2007).
29. Cen, C. *et al.* Nanoscale control of an interfacial metal–insulator transition at room temperature. *Nature Mater.* **7,** 298–302 (2008).
30. Xie, Y. W., Bell, C., Yajima, T., Hikita, Y. & Hwang, H. Y. Charge writing at the $LaAlO_3/SrTiO_3$ surface. *Nano Lett.* **10,** 2588–2591 (2010).
31. Hotta, Y., Susaki, T. & Hwang, H. Y. Polar discontinuity doping of the $LaVO_3/SrTiO_3$ interface. *Phys. Rev. Lett.* **99,** 236805 (2007).
32. Higuchi, T., Hotta, Y., Susaki, T., Fujimori, A. & Hwang, H. Y. Modulation doping of a Mott quantum well by a proximate polar discontinuity. *Phys. Rev. B* **79,** 075415 (2009).
33. Lanier, C. H. *et al.* Surface reconstruction with a fractional hole: $(\sqrt{5}\times\sqrt{5})$ *R*26.6° $LaAlO_3$ (001). *Phys. Rev. Lett.* **98,** 086102 (2007).

34. Takizawa, M. *et al.* Spectroscopic evidence for competing reconstructions in polar multilayers $LaAlO_3/LaVO_3/LaAlO_3$. *Phys. Rev. Lett.* **102,** 236401 (2009).
35. Freeland, J. W. *et al.* Charge transport and magnetization profile at the interface between the correlated metal $CaRuO_3$ and the antiferromagnetic insulator $CaMnO_3$. *Phys. Rev. B* **81,** 094414 (2010).
36. Pauli, S. A. *et al.* Evolution of the interfacial structure of $LaAlO_3$ on $SrTiO_3$. *Phys. Rev. Lett.* **106,** 036101 (2011).
37. Salluzzo, M. *et al.* Orbital reconstruction and the two-dimensional electron gas at the $LaAlO_3/SrTiO_3$ interface. *Phys. Rev. Lett.* **102,** 166804 (2009).
38. Pinta, C. *et al.* Suppression of spin-state transition in epitaxially strained $LaCoO_3$. *Phys. Rev. B* **78,** 174402 (2008).
39. Aruta, C. *et al.* Orbital occupation, atomic moments, and magnetic ordering at interfaces of manganite thin films. *Phys. Rev. B* **80,** 014431 (2009).
40. Okamoto, S. & Millis, A. J. Electronic reconstruction at an interface between a Mott insulator and a band insulator. *Nature* **428,** 630–633 (2004).
41. Pentcheva, R. & Pickett, W. E. Correlation-driven charge order at the interface between a Mott and a band insulator. *Phys. Rev. Lett.* **99,** 016802 (2007).
42. Chaloupka, J. & Khaliullin, G. Orbital order and possible superconductivity in $LaNiO_3/LaMO_3$ superlattices. *Phys. Rev. Lett.* **100,** 016404 (2008).
43. Hansmann, P. *et al.* Turning a nickelate Fermi surface into a cuprate-like one through heterostructuring. *Phys. Rev. Lett.* **103,** 016401 (2009).
44. Han, M. J., Marianetti, C. A. & Millis, A. J. Chemical control of orbital polarization in artificially structured transition-metal oxides: La_2NiXO_6 (X = B, Al, Ga, In) from first principles. *Phys. Rev. B* **82,** 134408 (2010).
45. Seo, S. S. A. *et al.* Two-dimensional confinement of $3d^1$ electrons in $LaTiO_3$-$LaAlO_3$ multilayers. *Phys. Rev. Lett.* **104,** 036401 (2010).
46. Benckiser, E. *et al.* Orbital reflectometry of oxide heterostructures. *Nature Mater.* **10,** 189–193 (2011).
47. Chakhalian, J. *et al.* Magnetism at the interface between ferromagnetic and superconducting oxides. *Nature Phys.* **2,** 244–248 (2006).
48. Chakhalian, J. *et al.* Orbital reconstruction and covalent bonding at an oxide interface. *Science* **318,** 1114–1117 (2007).
49. Yu, P. *et al.* Interface ferromagnetism and orbital reconstruction in $BiFeO_3$-$La_{0.7}Ca_{0.3}MnO_3$ heterostructures. *Phys. Rev. Lett.* **105,** 027201 (2010).
50. Jackeli, G. & Khaliullin, G. Spin, charge, and orbital order at the interface between correlated oxides. *Phys. Rev. Lett.* **101,** 216804 (2008).
51. Sai, N., Meyer, B. & Vanderbilt, D. Compositional inversion symmetry breaking in ferroelectric perovskites. *Phys. Rev. Lett.* **84,** 5636–5639 (2000).
52. Warusawithana, M. P., Colla, E. V., Eckstein, J. N. & Weissman M. B. Artificial dielectric superlattices with broken inversion symmetry. *Phys. Rev. Lett.* **90,** 036802 (2003).
53. Lee, H. N., Christen, H. M., Chisholm, M. F., Rouleau, C. M. & Lowndes, D. H. Strong polarization enhancement in asymmetric three-component ferroelectric superlattices. *Nature* **433,** 395–399 (2005).
54. Yamada, H., Kawasaki, M., Ogawa, Y. & Tokura, Y. Perovskite oxide tricolor superlattices with artificially broken inversion symmetry by interface effects. *Appl. Phys. Lett.* **81,** 4793–4795 (2002).
55. Ogawa, Y. *et al.* Nonlinear magneto-optical Kerr rotation of an oxide superlattice with artificially broken symmetry. *Phys. Rev. Lett.* **90,** 217403 (2003).
56. Kida, N. *et al.* Optical magnetoelectric effect of patterned oxide superlattices with ferromagnetic interfaces. *Phys. Rev. Lett.* **99,** 197404 (2007).
57. Yamada, H. *et al.* Engineered interface of magnetic oxides. *Science* **305,** 646–648 (2004).
58. Reyren, N. *et al.* Superconducting interfaces between insulating oxides. *Science* **317,** 1196–1199 (2007).
59. Caviglia, A. D. *et al.* Electric field control of the $LaAlO_3/SrTiO_3$ interface ground state. *Nature* **456,** 624–627 (2008).
60. Bell, C. *et al.* Dominant mobility modulation by the electric field effect at the $LaAlO_3/SrTiO_3$ interface. *Phys. Rev. Lett.* **103,** 226802 (2009).
61. Schooley, J. F. *et al.* Dependence of the superconducting transition temperature on carrier concentration in semiconducting $SrTiO_3$. *Phys. Rev. Lett.* **14,** 305–307 (1965).
62. Ahn, C. H., Triscone, J-M. & Mannhart, J. Electric field effect in correlated oxide systems. *Nature* **424,** 1015–1018 (2003).
63. Ueno, K. *et al.* Electric-field-induced superconductivity in an insulator. *Nature Mater.* **7,** 855–858 (2008).
64. Shimotani, H. *et al.* Insulator-to-metal transition in ZnO by electric double layer gating. *Appl. Phys. Lett.* **91,** 082106 (2007).
65. Yuan, H. T. *et al.* High-density carrier accumulation in ZnO field-effect transistors gated by electric double layers of ionic liquids. *Adv. Funct. Mater.* **19,** 1046–1053 (2009).
66. Ye, J. T. *et al.* Gate-induced interface superconductivity on an atomically flat film. *Nature Mater.* **9,** 125–128 (2010).
67. Bollinger, A. T. *et al.* Superconductor–insulator transition in $La_{2-x}Sr_xCuO_4$ at the pair quantum resistance. *Nature* **472,** 458–460 (2011).
68. Kozuka, Y. *et al.* Enhancing the electron mobility via delta-doping in $SrTiO_3$. *Appl. Phys. Lett.* **97,** 222115 (2010).
69. Jalan, B., Stemmer, S., Mack, S. & Allen, S. J. Two-dimensional electron gas in δ-doped $SrTiO_3$. *Phys. Rev. B* **82,** 081103 (2010).
70. Kozuka, Y. *et al.* Two-dimensional normal-state quantum oscillations in a superconducting heterostructure. *Nature* **462,** 487–490 (2009).
71. Kim, M. *et al.* Fermi surface and superconductivity in low-density high-mobility δ-doped $SrTiO_3$. *Phys. Rev. Lett.* **107,** 106801 (2011).
72. Caviglia, A. D. *et al.* Tunable Rashba spin-orbit interaction at oxide interfaces. *Phys. Rev. Lett.* **104,** 126803 (2010).
73. Shalom, M. B. *et al.* Tuning spin-orbit coupling and superconductivity at the $SrTiO_3/LaAlO_3$ interface: a magnetotransport study. *Phys. Rev. Lett.* **104,** 126802 (2010).
74. Dikin, D. A. *et al.* Coexistence of superconductivity and ferromagnetism in two dimensions. *Phys. Rev. Lett.* **107,** 056802 (2011).
75. Li, L., Richter, C., Mannhart, J. & Ashoori, R. C. Coexistence of magnetic order and two-dimensional superconductivity at $LaAlO_3/SrTiO_3$ interfaces. *Nature Phys.* **7,** 762–766 (2011).
76. Bert, J. A. *et al.* Direct imaging of the coexistence of ferromagnetism and superconductivity at the $LaAlO_3/SrTiO_3$ interface. *Nature Phys.* **7,** 767–771 (2011).
77. Michaeli, K., Potter, A. C. & Lee, P. A. Superconductivity and ferromagnetism in oxide interface structures: possibility of finite momentum pairing. Preprint at http://arXiv.org/abs/1107.4352 (2011).
78. Stormer, H. L. Nobel Lecture: the fractional quantum Hall effect. *Rev. Mod. Phys.* **71,** 875–889 (1999).
79. Tokura, Y. & Hwang, H. Y. Complex oxides on fire. *Nature Mater.* **7,** 694–695 (2008).
80. Tsukazaki, A. *et al.* Quantum Hall effect in polar oxide heterostructures. *Science* **315,** 1388–1391 (2007).
81. Tsukazaki, A. *et al.* Observation of the fractional quantum Hall effect in an oxide. *Nature Mater.* **9,** 889–893 (2010).
82. Schlom, D. G. & Pfeiffer L. N. Upward mobility rocks! *Nature Mater.* **9,** 881–883 (2010).
83. Kozuka, Y. *et al.* Insulating phase of a two-dimensional electron gas in $Mg_xZn_{1-x}O/ZnO$ heterostructures below ν = 1/3. *Phys. Rev. B* **84,** 033304 (2011).
84. Tanatar, B. & Ceperley, D. Ground state of the two-dimensional electron gas. *Phys. Rev. B* **39,** 5005–5016 (1989).
85. Tsukazaki, A. *et al.* Spin susceptibility and effective mass of two-dimensional electrons in Mg_xZn_{1-x}/ZnO heterostructures. *Phys. Rev. B* **78,** 233308 (2008).
86. De Poortere, E. P., Tutuc, E., Papadakis, S. J. & Shayegan, M. Resistance spikes at transitions between quantum Hall ferromagnets. *Science* **290,** 1546–1549 (2000).
87. Kroemer, H. Quasi-electric fields and band offsets: teaching electrons new tricks. Nobel Lecture, 8 December 2000; http://go.nature.com/5SFA6C
88. Waser, R. & Aono, M. Nanoionics-based resistive switching memories. *Nature Mater.* **6,** 833–840 (2007).
89. Sawa, A. Resistive switching in transition metal oxides. *Mater. Today* **11,** 28–36 (2008).
90. Nakamura, M., Sawa, A., Fujioka, J., Kawasaki, M. & Tokura, Y. Interface band profiles of Mott-insulator/Nb:$SrTiO_3$ heterojunctions as investigated by optical spectroscopy. *Phys. Rev. B* **82,** 201101 (2010).
91. Matsubara, M. *et al.* Photoinduced switching between charge and orbital ordered insulator and ferromagnetic metal in perovskite manganites. *Phys. Rev. B* **77,** 094410 (2008).
92. Kim, B. J. *et al.* Novel $J_{\rm eff}$=1/2 Mott state induced by relativistic spin–orbit coupling in Sr_2IrO_4. *Phys. Rev. Lett.* **101,** 076402 (2008).
93. Datta, S. & Das B. Electronic analog of the electro-optic modulator. *Appl. Phys. Lett.* **56,** 665–667 (1990).
94. Chernyshov, A. *et al.* Evidence for reversible control of magnetization in a ferromagnetic material by means of spin–orbit magnetic field. *Nature Phys.* **5,** 656–659 (2009).
95. Miron, I. M. *et al.* Current-driven spin torque induced by the Rashba effect in a ferromagnetic metal layer. *Nature Mater.* **9,** 230–234 (2010).
96. Kimura, T. *et al.* Magnetic control of ferroelectric polarization. *Nature* **426,** 55–58 (2003).
97. Katsura, H., Nagaosa, N. & Balatsky, A. V. Spin current and magnetoelectric effect in noncollinear magnets. *Phys. Rev. Lett.* **95,** 057205 (2005).
98. Onoda, M. & Nagaosa, N. Quantized anomalous Hall effect in two-dimensional ferromagnets: quantum Hall effect in metals. *Phys. Rev. Lett.* **90,** 206601 (2003).
99. Hasan, M. Z. & Kane, C. L. Topological insulators. *Rev. Mod. Phys.* **82,** 3045–3067 (2010).
100. Qi, X. L. & Zhang, S. C. Topological insulators and superconductors. *Rev. Mod. Phys.* **83,** 1057–1110 (2011).
101. Xiao, D., Zhu, W., Ran, Y., Nagaosa, N. & Okamoto, S. Interface engineering of quantum Hall effects in digital transition-metal oxide heterostructures. *Nature Commun.* **2,** 596 (2011).

102. Smadici, S. *et al.* Electronic reconstruction at $SrMnO_3$–$LaMnO_3$ superlattice interfaces. *Phys. Rev. Lett.* **99,** 196404 (2007).
103. Logvenov, G., Gozar, A. & Bozovic, I. High-temperature superconductivity in a single copper-oxygen plane. *Science* **326,** 699–702 (2009).
104. Smadici, S. *et al.* Superconducting transition at 38 K in insulating-overdoped La_2CuO_4-$La_{1.64}Sr_{0.36}CuO_4$ superlattices: evidence for interface electronic redistribution from resonant soft X-ray scattering. *Phys. Rev. Lett.* **102,** 107004 (2009).
105. May, S. J. *et al.* Magnetically asymmetric interfaces in a ($LaMnO_3$)/($SrMnO_3$) superlattice due to structural asymmetries. *Phys. Rev. B* **77,** 174409 (2008).
106. Boris A. V. *et al.* Dimensionality control of electronic phase transitions in nickel-oxide superlattices. *Science* **332,** 937–940 (2011).

Acknowledgements

This work was partly supported by the Japan Society for the Promotion of Science (JSPS) through its Funding Program for World-Leading Innovative R&D on Science and Technology (FIRST Program). H.Y.H. acknowledges support from the Department of Energy, Office of Basic Energy Sciences, under contract DE-AC02-76SF00515. B.K. acknowledges support by the German Science Foundation under collaborative Grant No. SFB/TRR80. N.N. acknowledges support by MEXT Grand-in-Aid No. 20740167, 19048008, 19048015, 21244053, and the Strategic International Cooperative Program (Joint Research Type) from the Japan Science and Technology Agency.

Additional information

The authors declare no competing financial interests. Correspondence and requests for materials should be addressed to H.Y.H. or Y.T.